

Research article

Body segment inertial parameters of elite swimmers using DXA and indirect methods

Marcel Rossi ✉, Andrew Lyttle, Amar El-Sallam, Nat Benjanuvatra and Brian Blanksby

School of Sport Science, Health & Exercise Science, The University of Western Australia, Crawley, Australia

Abstract

As accurate body segment inertial parameters (BSIPs) are difficult to obtain in motion analysis, this study computed individual BSIPs from DXA scan images. Therefore, by co-registering areal density data with DXA grayscale image, the relationship between pixel color gradient and the mass within the pixel area could be established. Thus, one can calculate BSIPs, including segment mass, center of mass (COM) and moment of inertia about the sagittal axis (I_{xx}). This technique calculated whole body mass very accurately (%RMSE of < 1.5%) relatively to results of the generic DXA scanner software. The BSIPs of elite male and female swimmers, and young adult Caucasian males ($n = 28$), were computed using this DXA method and 5 other common indirect estimation methods. A 3D surface scan of each subject enabled mapping of key anthropometric variables required for the 5 indirect estimation methods. Mass, COM and I_{xx} were calculated for seven body segments (head, trunk, head + trunk, upper arm, forearm, thigh and shank). Between-group comparisons of BSIPs revealed that elite female swimmers had the lowest segment masses of the three groups ($p < 0.05$). Elite male swimmers recorded the greatest inertial parameters of the trunk and upper arms ($p < 0.05$). Using the DXA method as the criterion, the five indirect methods produced errors greater than 10% for at least one BSIP in all three populations. Therefore, caution is required when computing BSIPs for elite swimmers via these indirect methods, DXA accurately estimated BSIPs in the frontal plane.

Key words: Body segment inertial parameters, DXA, indirect estimation methods, swimming.

Introduction

Technological improvements in computer storage, processing and simulation; and camera resolution and acquisition frequency in recent years allow a greater understanding of swimming biomechanics. For instance, studies in Computer Fluid Dynamics (CFD) have explored how the external forces (propulsive and drag) are generated by the water medium as a result of the body kinematics underwater (Bixler and Schloder, 1996; Lyttle and Keys, 2006; Marinho et al., 2009). Also, a video-based Markerless Motion Capture (MMC) approach has been proposed as an alternative for more reliable and less time-consuming kinematic analyses of swimming (Ceseracciu et al., 2011).

However, to estimate joint kinetics and internal forces (e.g., muscle, tendon and bone contact forces), and understand how they influence swimming performance and injury onset, accurate body segment inertial parameters (BSIP) data also are necessary. These inertial parameters are segment mass, center of mass (COM), and princi-

pal moments of inertia about the longitudinal (I_{yy}), sagittal (I_{xx}) and transverse axes (I_{zz}), passing through the COM. Several BSIP estimation methods have been established and are classified as either direct (i.e., BSIPs measured directly from cadavers, or medical imaging technology with living subjects) or indirect (i.e., BSIPs estimated from specific anthropometric values).

Early BSIP estimations in living subjects used models developed from direct measurements from a few cadavers of elderly Caucasian males (Chandler et al., 1975; Clauser et al., 1969; Dempster, 1955). Extrapolating those data to other populations is restrictive due to their different body morphologies. Also, fluid and tissue loss in segmentation, and different properties of living and deceased tissue, can affect the accuracy of derived BSIP information (Durkin, 2008).

Currently, direct measurement of BSIPs on living humans is possible using medical imaging technologies such as gamma-ray scanning (Zatsiorsky and Seluyanov, 1983; Zatsiorsky et al., 1990), computed tomography imaging (CT) (Ackland et al., 1988; Huang and Suarez, 1983) and magnetic resonance imaging (MRI) (Cheng et al., 2000; Martin et al., 1989; Mungiole and Martin, 1990). Although accurate, they are not widely used in biomechanics due to expense, labor demands during data processing, limited accessibility and/or exposure of subjects to high doses of radiation.

Indirect estimations of BSIPs are based on relationships between anthropometric variables and the required inertial parameters. They can be either regression equations or geometrical models. Regression equations use an individual's anthropometric data BSIPs predictors (Chandler et al., 1975; Dempster, 1955; Durkin and Dowling, 2003; Zatsiorsky and Seluyanov, 1983; 1985). In contrast, the geometric model approach creates and uses geometric figure templates for the segments derived from anthropometry. Then, BSIPs are calculated from the geometric formulae (Durkin and Dowling, 2006; Hanavan Jr, 1964; Yeadon, 1990; Zatsiorsky et al., 1990). As anthropometry can be gathered quickly, at low cost and without the risk of radiation exposure, indirect methods are more practical and widely adopted when assessing human motion. Despite these advantages, indirect estimations contain some errors, particularly when applied to subjects physically different from the sample used to devise the indirect method (Durkin and Dowling, 2003).

Dual-energy X-ray absorptiometry (DXA) is a recent medical-imaging technique with potential for direct measurement of BSIPs in living subjects. It is similar to gamma-ray scanning as it relies on the attenuation of

radiation beams passing through the body to measure surface density. The main difference is that DXA uses two X-ray intensities which allow measurement of bone mineral and soft tissue masses separately (the latter includes fat and lean tissue masses (Ellis, 2000; Laskey, 1996) Hence, it is used primarily to determine bone mineral density and body composition *in vivo* (Ellis, 2000; Fuller et al., 1992; Haarbo et al., 1991; Laskey, 1996; Mazess et al., 1990). Recently, it has been used to estimate segment mass, COM position in the frontal plane, and I_{xx} (Durkin et al., 2002; Ganley and Powers, 2004a; Wicke and Dumas, 2008). Using DXA is accurate, non-invasive, low cost, emits low radiation, and is faster to analyze than gamma-ray scanning and other imaging methods (Durkin et al., 2002; Ganley and Powers, 2004b; Wicke and Dumas, 2008).

Sport performance analyses of specific athlete populations demand precision because 0.01 s time improvement or a minor technique alteration can be the difference between winning and losing. It has been demonstrated that morphologies of elite athletes tend to be optimized specifically for the sport in which they participate (Olds and Tomkinson, 2009). Thus, considerable anatomical variations are found between athletes from different sports and the general population; which, in turn, may lead to significant differences in BSIPs of these populations. Therefore, indirect BSIP estimation methods derived from small, non-sport-specific groups may not be sufficient to calculate accurate BSIPs for elite athletes. While inaccurate BSIPs can create errors, the errors incurred when using indirect methods is not known.

Therefore, this study examined whether there were significant differences in BSIPs measured with DXA between elite male swimmers, elite female swimmers and/or young adult Caucasian males. Also, errors associated with computing BSIPs for these three populations were quantified by using five indirect estimation methods that are commonly used in assessing human motion. It was hypothesized that greater errors would be observed between elite swimmers than in normal Caucasian males. This was because the elite swimmers were likely to record a sport-specific body morphology and proportions; whereas the Caucasian male sample was selected to match the sample used by Zatsiorsky and colleagues when developing three of the indirect methods (Zatsiorsky and Seluyanov, 1983; Zatsiorsky et al., 1990).

Methods

Participants

Ten competitive male swimmers (age 26.17 ± 3.96 yrs, height 1.86 ± 0.09 m, weight 81.16 ± 9.30 kg), 8 competitive female swimmers (age 21.13 ± 5.85 yrs, height 1.73 ± 0.07 m, weight 61.69 ± 5.47 kg), and a group of 10 healthy, young adult Caucasian males who were Sport Science university students, non-swimmers, acted as subjects. All swimmers had achieved at least one qualifying standards for the Australian Swimming Championships at the time of the research (a number of swimmers also had international competition experience, or held Olympic and World Championship titles and records).

The sport science student group had similar anthropometric profiles as subjects in the studies by Zatsiorsky et al. (Zatsiorsky and Seluyanov, 1983; 1985; Zatsiorsky et al., 1990); and this can be verified in Table 1. The resemblance was also assessed through a series of one-sample t-tests that determined whether segment masses of the current participants were different from those found in the above Zatsiorsky studies.

Table 1. Mean (SD) of the age (years), height (cm) and weight (Kg) of young adult Caucasian males in the cohort of the present study (DXA, n=10) and in the studies of Zatsiorsky et al. (1983, 1985, 1990; n=100)

Cohort	Age	Height	Weight
DXA (n = 10)	22.5 (4.8)	1.77 (.08)	74.9 (8.7)
Zatsiorsky et al. (n = 100)	23.8 (6.2)	1.74 (.06)	73.0 (9.1)

Approval was obtained from The University of Western Australia Human Research Ethics Committee. Information regarding the procedures and possible risks was distributed to all participants, who provided written informed consent prior to testing.

Indirect BSIP estimation methods

The BSIPs derived from DXA were compared with those gathered from the five indirect BSIP estimation methods. Two methods were based on cadaver data (Chandler et al., 1975, Yeadon, 1990) and three others used data from living subjects (Zatsiorsky, 1983; 1985; Zatsiorsky et al., 1990). These were chosen because they are regularly used in biomechanical analyses, and they provide moments of inertia in all of the orthogonal planes. For the most part, they enabled the same body segmentation protocol for the following segments: head, trunk, upper arm, forearm, hands, thighs, shanks and feet (feet and hands were excluded in this study). When necessary, estimation methods were modified to minimize variations due to different segmentation protocols; and to facilitate using anthropometric measures derived from the standard protocol established by the International Society for Advancement of Kinanthropometry (ISAK) (Olds and Tomkinson, 2009).

The five indirect estimation methods were:

1. The Modified Chandler method (C) (Chandler et al., 1975). This method uses simple linear relationships between the total body weight and separate segment masses; with the COM position as a fixed ratio of the distance from the COM to the proximal joint of the segment, and the length of the segment (Chandler et al., 1975). I_{xx} was determined by using the non-linear equations from Yeadon and Morlock (1989).

2. The Modified Yeadon method (Y) (Yeadon, 1990). This is a geometric method using cylindrical and stadium-shaped solids to represent body segments. To calculate BSIPs, the geometrical shapes are assigned a uniform density value based on Dempster's data (Dempster, 1955). Then, the mass, COM and I_{xx} of each solid were computed from the provided equations (Yeadon, 1990). Modifications to the original method were carried out to ensure that the segmentation protocol used in this method closely matched the protocol adopted in our DXA method, as explained below.

3. The Zatsiorsky Simple Regression Method (Z1) was proposed by Zatsiorsky and Seluyanov (1983). This regression uses only the whole body mass and height as predictors for each of the BSIPs.

4. The Zatsiorsky Multiple Regression Model (Z2) (Zatsiorsky and Seluyanov, 1985). This regression model requires up to 4 local anthropometric measures (i.e., segment lengths, breadths, girths and diameters) of each segment as predictors in the linear equations. The underlying principle of this technique is the notion that inertial parameters of a given segment should correlate better with the anthropometry of that segment rather than global measures such as body weight.

5. The Zatsiorsky Geometrical Model (Z3) (Zatsiorsky, Seluyanov and Chugunova, 1990). Under the assumption that each segment can be represented as a circular cylinder, this method uses a segment-specific, quasi-density value calculated to minimize differences between the cylinder and the real segment volumes. Zatsiorsky et al. (1990) claimed that this geometric model can estimate the BSIPs of groups not necessarily matching the anthropometry of the cohort used to derive the equations.

Data acquisition Protocol

Participants underwent a full body DXA scan and 3D surface scan while wearing Fédération Internationale de Natation (FINA) approved swimming suits and caps. Participants had 22 spherical markers (20 mm diameter) made from glass marbles attached to specific body landmarks prior to the above scans (Table 2). These markers were placed to appear outside the boundary of the body on the DXA output image. Glass was chosen for the markers because its density was different from bone mineral and other body tissues ($\sim 3\text{g/cm}^3$) and could be identified easily on the DXA output image.

Table 2. Glass marble naming and locations

Segment / Joint	Label	Location
Head	L/R FHD	Front head marker
Shoulder joint	L/R ACR	The midpoint on the acromion process lateral ridge
Elbow joint	L/R MEL	Medial epicondyle of the humerus
	L/R LEL	Lateral epicondyle of the humerus
Wrist joint	L/R AMWR	Anterior mid-styilion
	L/R PMWR	Posterior mid-styilion
Trunk	L/R ICP	Tubercle of the iliac crest
Knee joint	L/R MKN	Medial epicondyle of the femur
	L/R LKN	Lateral epicondyle of the femur
Ankle joint	L/R MAN	Medial malleolus of the tibia
	L/R LAN	Lateral malleolus of the tibia

Dual-Energy X-Ray Absorptiometry (DXA)

The GE Lunar Prodigy DXA scanner (GE Healthcare, Madison, WI, USA) projected two X-ray beams of different intensities onto each subject's body. Based on the attenuation of the energies as they pass through the body, the scanner can evaluate the areal density (i.e., mass per area unit in the frontal plane) and the mass associated

with each compartment (i.e., bone mineral, lean tissue and fat tissue).

The subjects assumed supine positions with the feet spaced shoulder-width apart, and the forearms and hands assumed a relaxed, 90° pronated position (palms facing thighs). This position ensured that the anatomical sagittal plane was as close to parallel to the scan table as possible, and the subjects fitted within the 60-cm wide scanning area. The whole body was scanned once in a process that took approximately 5 minutes and exposed the subject to a radiation dose of $\sim 0.8 \mu\text{Sv}$.

3D Body Laser Scan

An Artec LTM 3D scanner (Artec, TDSL, Moscow, Russia) was used to create a surface scan of each participant. From these, the anthropometric measures and joint center positions were calculated (Figure 1). A light projector emitted a mesh of dots onto the body surface, and a video camera to capture images of the projected dots (3D frames). Both the camera and projector were calibrated relative to each other (raster-stereography). According to the manufacturer, the scanner has a 3D resolution of up to 1.0 mm, 3D point accuracy of up to 0.2 mm, and a maximal capture rate of 15 frames per second. The Artec 3D Scanner v0.6 software was used to operate the scanner, and capture and process the scanned data.



Figure 1. The Artec LTM 3D scanner.

Prior to scanning, 28 additional spherical wooden markers (20 mm diameter) were strategically placed on the body (Table 3) to combine with the glass markers and create the anatomical coordinate system (ACS) for each body segment. To avoid excessive sway during scanning, subjects looked at a fixed point on the wall ahead and rested their fingers on two nearby tripods. The first scanning phase covered the head, trunk and upper limbs; and the second scan, the lower limbs (Figure 2).

The post-processing was also conducted using the Artec 3D Scanner v0.6 software. The software enabled finer alignment of the 3D frames, smoothness of the surface, filling the surface holes, discarding of unwanted objects and the creation of the single polygonal 3D model of the whole body (i.e., representation of the body surface using a triangulation grid).

Anthropometry

Heights, lengths, breadths and girths were taken from all subjects' 3D scans for input into the indirect BSIP estimation method equations. Anthropometry from 3D scans had shown high validity and reproducibility (Lu and Wang,

Table 3. 3D scan marker naming convention and locations.

Segment / Joint	Label	Location
Head	L/R BHD	Back head marker
Shoulder joint	L/R Acr1	Acromion triad: posterior marker
	L/R Acr2	Acromion triad: central-medial marker
	L/R Acr3	Acromion triad: posterior marker
		The rigid bar between Acr1 and Acr3 runs parallel with the lateral ridge of the acromion
Wrist joint	L/R MWR	Styloid process of the ulna
	L/R LWR	Styloid process of the radius
Hand	L/R Hand1	2 nd carpo-metacarpal joint
	L/R Hand2	5 th carpo-metacarpal joint
	L/R Hand3	Head of the 3 rd metacarpal
Trunk	C7	Spinous process of the 7 th cervical vertebra
	IJ	Deepest point of the incisura jugularis (suprasternale)
	XP	Xiphoid process
	Nav	Navel
		L/R ASIS Anterior superior iliac spine
		L/R PSIS Posterior superior iliac spine
Foot	L/R Foot1	Calcaneus
	L/R Foot2	Head of the 1 st metatarsal
	L/R Foot3	Head of the 5 th metatarsal

2008). When possible, measures followed the definitions of ISAK; and the Laboratory Standards Assistance Scheme of the Australian Sports Commission (Olds and Tomkinson, 2009).



Figure 2. The 3D scan of a participant after the scanning procedure (before post-process)

Biomechanical model

A 16-segment biomechanical model (head, upper trunk, middle trunk, lower trunk, upper arms, forearms, hands, thighs, shanks and feet) was devised so that all BSIP estimation methods could be fitted easily to the model. A model of every subject was created using the 3D coordinates of the markers obtained with the Artec 3D Scanner v0.6 software.

The ACS of the upper and lower limb segments were created following recommendations from the International Society of Biomechanics (Lu and Wang, 2008; Wu et al., 2005). The ankle, wrist and shoulder (glenohumeral) joint centers were determined according to the UWA biomechanical model (Besier et al., 2003; Campbell et al., 2009; Chin et al., 2010). The elbow and knee joint centers were defined as midway between the medial and the lateral epicondyles, of the humerus and femur, respectively. Regression equations were used for the hip joint center and a whole trunk coordinate system was created according to de Leva (1996). The long axis of the whole trunk was used also for the head segment.

Data processing

Previous studies used the linear relationship between the attenuation coefficients of the high energy beams, and each was recorded in rectangular elements that formed the scan area matrix and the mass of a given phantom (Durkin et al., 2002, Wicke and Dumas, 2008). As the code needed for calculating the mass for each rectangular element was unavailable, the raw data were accessed via an ACSII code de-compiler (Dowling, personal correspondence, 2011). A unique aspect of this study was that mass data were extracted directly from the generic DXA enCORE[®] software (version 8.50.093, GE Healthcare, 2004) made available from the manufacturer for this research. The GE Healthcare enCORE[®] software displayed two different data matrices of which the first provided mass data for the bone mineral compartment (BMD). The second provided mass data for the tissue compartment (TISSUE), which consisted of extracellular fluids and solids, total body water, intracellular solids and fat (St-Onge et al., 2004). Each matrix was divided into rectangular elements with dimensions of 0.51 cm x 1.54 cm in the transverse (x) and longitudinal (y) directions, respectively; and referred to as mass elements. Hence, each element represented a section within the entire scanned area, and the summation of both matrices provided the whole body mass.

The enCORE[®] software showed the coordinates and mass value of each mass element on the bottom of the screen, when the mouse cursor is over an area of the scan image (Figure 3). This worked for both the BMD and the TISSUE images, but the data matrices could not be exported and saved in any other formats for further processing. To extract mass data manually (i.e. by moving the mouse cursor from one mass element to the next, and then record the values externally) was not practical. Therefore, data from the two matrices were co-registered with their respective grayscale images (8-bits bitmap files, resolution of 72 DPI) exported by the scanner software (Figure 3) using a code written in Matlab[®] (Ver. 7.8.0.347) (Rossi et al., 2012). The images created were based on the coefficients of attenuation that were measured. This should result in a linear relationship between the shade of

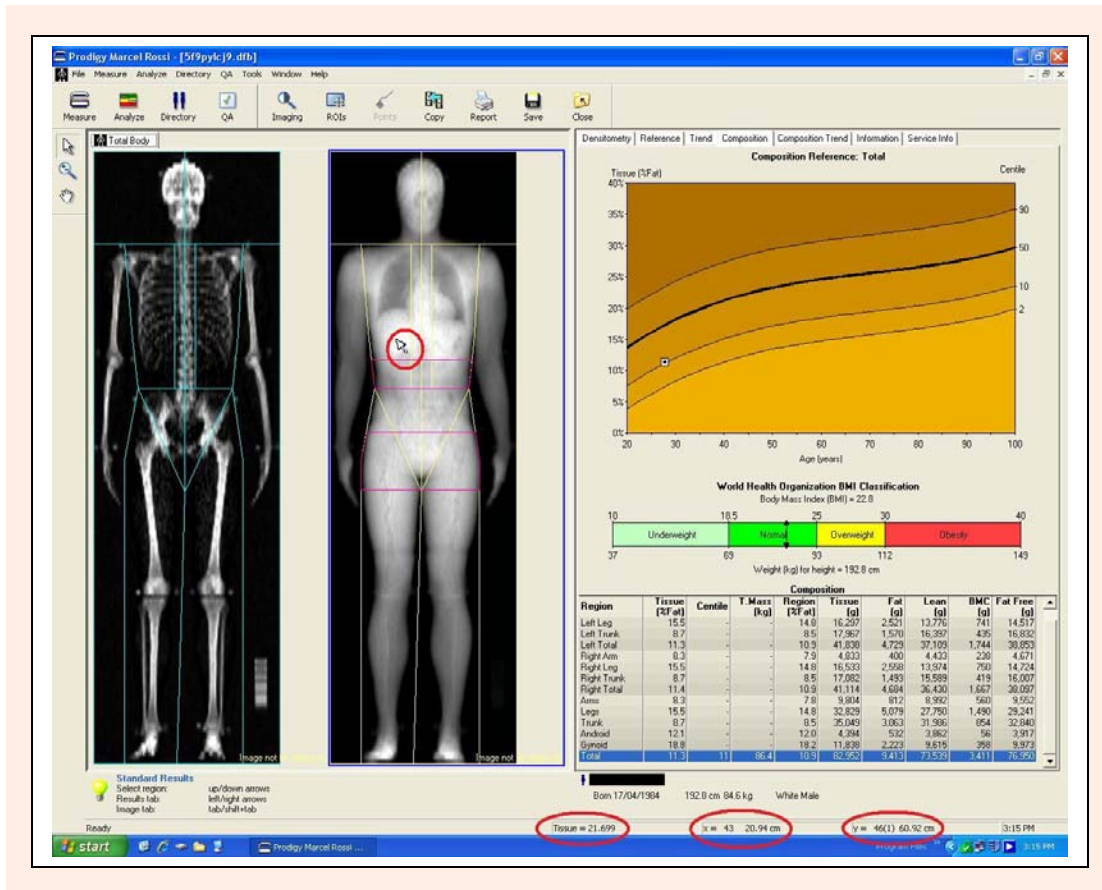


Figure 3. Screenshot of the enCORE® software showing the two BMD and TISSUE images derived from the respective matrices. When the mouse is placed on a given area (red circle), the mass and the coordinates the local mass element pointed to by the arrow, are shown on the bottom of the screen (red ellipses).

a given pixel of the image, and the areal density of the region represented by the pixel (i.e., the whiter the shade of the pixel, the greater the amount of mass referred to that area). The whole process is described in Rossi et al. (2012).

The method was validated by comparing the whole body mass, tissue mass and bone mineral mass values calculated by the enCORE® software (GE Corporation); with those calculated by summing all pixel masses for the 28 subjects. The minimum (E_{min}) and maximum (E_{max}) errors expressed in kilograms (kg) were computed using the enCORE® values as criteria. The mean absolute percentage errors (MAPE) and the percentage root mean square errors (%RMSE), were calculated as:

$$MAPE = \sum \left(\frac{|M_R - M_M|}{M_R} \right) \times \frac{100}{N} \quad \text{Equation 1}$$

$$\%RMSE = \sqrt{\frac{\sum (M_R - M_M)^2}{N}} \times 100 \quad \text{Equation 2}$$

Where M_R and M_M are the real mass value from the scanner and summing all pixel masses, and N is the number of subjects.

Another Matlab code (Rossi, 2012) was created to divide the scan image into a 16-segment model (head, upper trunk, middle trunk, lower trunk, upper arm, forearm, hands, thighs, shanks and feet); and to calculate the

mass (M_S , kg), COM position (cm) on the longitudinal axis of the segment (as a distance from the distal end point of the segment); and I_{xx} ($kg \cdot cm^2$, assuming all sagittal axes were perpendicular to the scanning plane) of each segment using the protocol of Zatsiorsky and Seluyanov (1983). This function used body landmark coordinates as input to determine the joint centers and sectioning planes (Figure 4). Those coordinates were entered when clicking on the bone landmarks viewed in the BMD image. Extra clicked points also were used to define vertices of a geometric figure within which the segment was placed; and, outside which, all the mass pixels were excluded from the calculations (Figure 5). Coordinates of the elbow, wrist, knee and ankle joint centers were calculated, and the same points used to define those joint centers, also defined the segmentation plane (perpendicular to the scanning plane). The shoulder and hip joint centers were obtained by clicking on the regions of the BMD image that represented the centers of the heads of the humerus and femur bones. The segmentation plane of the shoulder was defined by the line linking the acromion landmark to the armpit. The segmentation plane of the hip was defined by a line passing over the hip joint center at an angle of 37° to the longitudinal axis of the trunk (i.e., a line linking the midpoint between the hips and the midpoint between the shoulders).

The M_S , COM and I_{xx} were computed for each segment by using the following equations (Durkin et al.,

2002):

$$M_S = \sum m \tag{Equation 3}$$

$$CoM = \left[\frac{\sum xm}{M_S} \quad \frac{\sum ym}{M_S} \right] \tag{Equation 4}$$

$$I_{xx} = \sum mr^2 \tag{Equation 5}$$

Where *x* and *y* are the coordinates of the pixel mass, *m* is the mass value of each pixel mass, and *r* is the distance from the pixel mass to the segment COM (radius of gyration).

Data analysis

The mean percentage error of each indirect estimation method was calculated for each subject group. A 5 X 3 (indirect estimation method X subject group) mixed-model analysis of variance (SPANOVA, $\alpha=0.05$) of the percentage errors was conducted for each segment and for each inertial parameter. This was followed by a Tukey-HSD post-hoc analysis to determine whether there were any differences between estimation methods, between swimmers and normal Caucasian males, and possible interactions between independent variables. It was hypothesized that any errors found for the two groups of swimmers would be significantly greater than those found among the cohort resembling the studies by Zatsiorsky et al. (Zatsiorsky and Seluyanov, 1983; 1985; Zatsiorsky et al., 1990). This was hypothesized, regardless of segments or inertial parameters, because the methods Z1, Z2 and Z3 were derived from a similar population of young adult Caucasian males; whereas C and Y, even though derived from a few elderly cadaver males, supposedly would resemble that cohort rather than the elite swimmers.

In addition, the root mean square error was calculated for each of the five indirect BSIP estimation methods, and applied to elite male and female swimmers. Any significant differences which occurred in absolute errors

of indirect BSIP estimation methods; when applied to elite male swimmers, elite female swimmers, and young adult Caucasian males, also were determined.

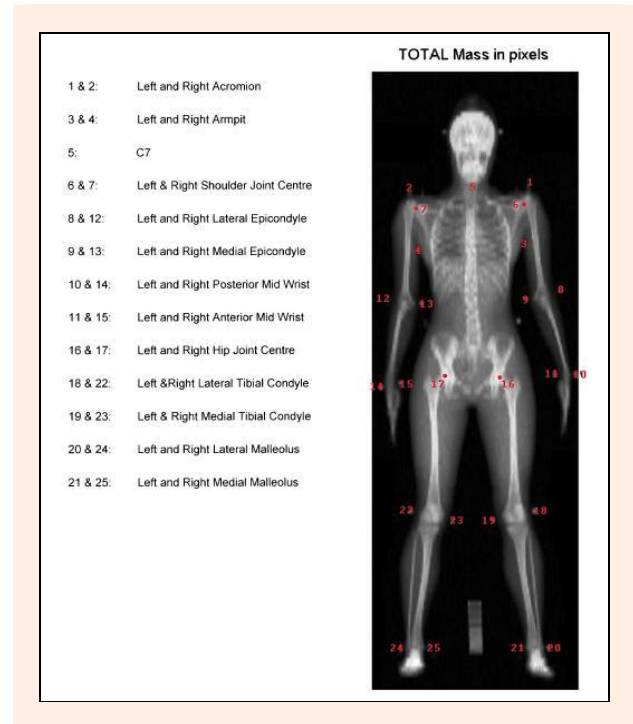


Figure 4. Representation of the 25 points used to segment the body.

Results

The errors associated with using the DXA methods are reported in Table 4. While large MAPE and %RMSE could be observed for the bone mineral mass, it had little influence on total mass prediction. But, in contrast, tissue mass was estimated with marginal errors.

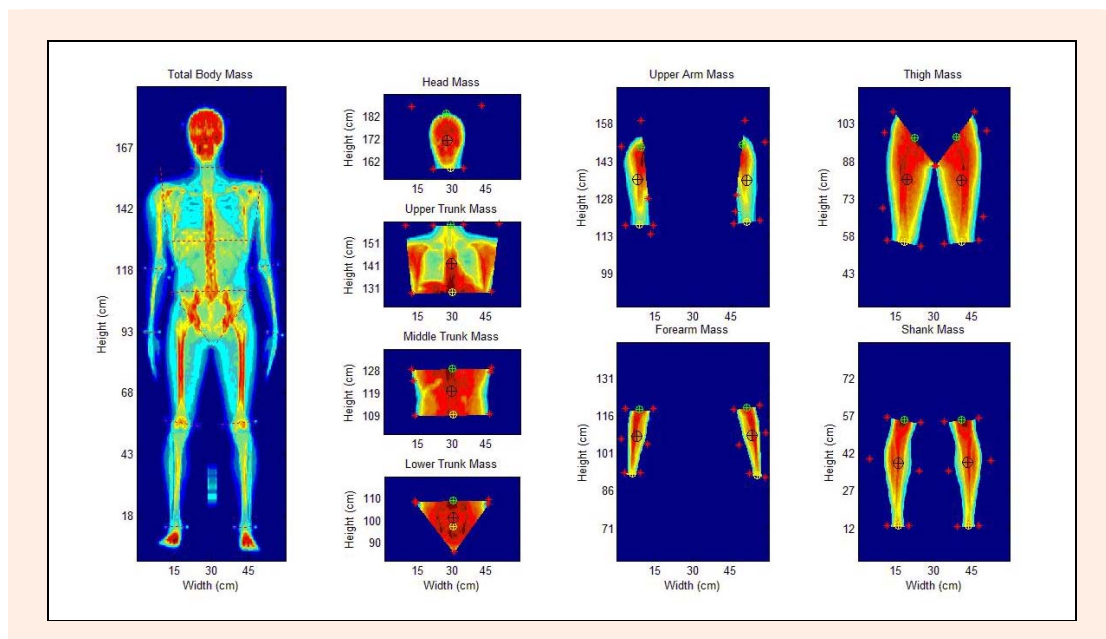


Figure 5. Segmentation planes in the whole body (left figure, red dashed line), the clicked points that defined the geometric figure used as frontier to delimit the segments (red dots), and the segment COM positions.

Table 4. Minimum error (E_{min} , Kg), Maximum error (E_{max} , Kg), Mean Absolute Percentage Error (MAPE, %) and Percentage Root Mean Square Error (%RMSE) for the bone mineral, tissue and whole body masses calculated from the respective images.

Compartment	E_{min}	E_{max}	MAPE	%RMSE
Bone mineral	.04	.60	9.32%	10.55%
Tissue	.09	1.72	1.09%	1.27%
Total	.01	2.12	1.18%	1.45%

Table 5. Mean (SD) segment masses (kg) of young adult Caucasian males tested in the present study (DXA, $n = 10$) and the young adult Caucasian males from Zatsiorsky studies (Zatsiorsky, $n = 100$).

Segment	Mass	
	DXA	Zatsiorsky
Head	4.99 (.50)	5.02 (.39)
Trunk*	34.08 (2.57)	31.77 (3.24)
Upper arm*	2.30 (.33)	1.98 (.32)
Forearm	1.20 (.16)	1.18 (.16)
Thigh*	9.69 (1.15)	10.36 (1.57)
Shank*	3.46 (.44)	3.16 (.44)

* $p < 0.05$ between DXA and Zatsiorsky

10 young adult males. These results were compared with the segment masses of the subjects in Zatsiorsky and Seluyanov (Zatsiorsky and Seluyanov, 1983). The ‘Zatsiorsky’ studies (Zatsiorsky and Seluyanov, 1983; 1985; Zatsiorsky et al., 1990) presented segment lengths as distances between bony landmarks rather than between joint centers. Moreover, rather than the absolute value of the I_{xx} or the radii of gyrations, they presented the radii of gyration as percentages of the segmental lengths. Therefore, similar comparisons for COM and I_{xx} are not provided, as the values could not be computed in

the same way. A series of one-sample t-tests was used to determine whether segment masses of the current participants were different from those found by Zatsiorsky et al. (Zatsiorsky and Seluyanov, 1983; 1985; Zatsiorsky et al., 1990). All segments except the head ($t = -0.20$, $p = 0.84$) and forearm ($t = 0.51$, $p = 0.61$) showed significant differences.

Tables 6, 7 and 8 show the means and SD for mass, COM and I_{xx} , for each of the estimation methods and subject groups. Despite some variations, comparisons between the mean values obtained from DXA and the other estimation methods did not reveal them to be statistically significant ($p > 0.05$).

The ANOVA revealed significant differences in the BSIP data between groups except for the head COM ($F(2,25) = 0.80$, $p = .46$) and thigh COM ($F(2,53) = 1.21$, $p = 0.31$). Female swimmers had significantly lower mass values for all segments than the other two groups (head: $F(2,25) = 8.90$; trunk: $F(2,25) = 27.03$; head plus trunk: $F(2,25) = 25.68$; upper arm: $F(2,53) = 19.27$; forearm: $F(2,53) = 28.91$; thigh: $F(2,53) = 10.41$; shank: $F(2,53) = 10.87$), forearm I_{xx} ($F(2,53) = 11.64$) and thigh I_{xx} ($F(2,53) = 5.78$). Male swimmers had significantly greater values than the other two groups for all parameters of the trunk (mass: $F(2,25) = 27.06$; COM: $F(2,25) = 39.27$; I_{xx} : $F(2,25) = 26.49$), head + trunk (mass: $F(2,25) = 25.68$; COM: $F(2,25) = 25.19$; I_{xx} : $F(2,25) = 22.13$), and upper arm (mass: $F(2,53) = 19.27$; COM: $F(2,53) = 5.08$; I_{xx} : $F(2,53) = 14.14$). Also, the male swimmers recorded significantly larger forearm COM values ($F(2,53) = 7.43$), greater head I_{xx} ($F(2,25) = 5.94$), shank COM values ($F(2,53) = 5.46$) and shank I_{xx} ($F(2,53) = 7.04$) than female swimmers.

Table 6. Mean (SD) segment mass (Kg) calculated for adult Caucasian male ($n = 10$), male swimmers ($n = 10$) and female swimmers ($n = 8$).

Segment	Group	Estimation Method					
		C	Y	Z1	Z2	Z3	DXA
Head	Adult male	4.34 (.22)	4.96 (.92)	5.13 (.23)	6.07 (.76)	5.74 (.76)	4.99 (.50)
	Male swimmers	4.54 (.29)	5.04 (.65)	5.35 (.26)	6.37 (.67)	5.71 (.68)	5.18 (.37)
	Female swimmers	3.92 (.16)	3.79 (.53)	4.85 (.18)	5.66 (.35)	4.91 (.58)	4.40 (.30)
Trunk	Adult male	39.72 (3.64)	34.10 (3.29)	33.02 (2.95)	36.05 (3.07)	32.07 (2.61)	34.08 (2.57)
	Male swimmers	43.04 (4.89)	38.91 (4.46)	35.55 (4.20)	37.68 (3.72)	36.52 (3.96)	39.14 (4.02)
	Female swimmers	32.80 (2.58)	27.48 (2.54)	26.71 (2.03)	31.52 (2.70)	26.02 (2.43)	28.45 (2.09)
Head + Trunk	Adult male	44.06 (3.86)	39.06 (4.00)	38.15 (3.16)	42.12 (3.46)	37.81 (3.20)	39.07 (2.97)
	Male swimmers	47.57 (5.18)	43.95 (5.06)	40.91 (4.44)	44.05 (3.92)	42.23 (4.35)	44.32 (4.34)
	Female swimmers	36.72 (2.74)	31.27 (2.94)	31.57 (2.19)	37.18 (2.84)	30.93 (2.65)	32.85 (2.28)
Upper arm	Adult male	2.09 (.14)	2.41 (.38)	2.06 (.18)	2.54 (.29)	2.25 (.37)	2.30 (.33)
	Male swimmers	2.21 (.19)	2.87 (.46)	2.23 (.25)	2.85 (.30)	2.55 (.41)	2.61 (.42)
	Female swimmers	1.84 (.09)	2.08 (.22)	1.68 (.13)	2.27 (.19)	1.78 (.20)	1.91 (.19)
Forearm	Adult male	1.27 (.12)	1.26 (.20)	1.21 (.09)	1.35 (.17)	1.20 (.26)	1.20 (.16)
	Male swimmers	1.37 (.16)	1.42 (.26)	1.30 (.12)	1.48 (.24)	1.32 (.25)	1.31 (.20)
	Female swimmers	1.05 (.08)	1.04 (.16)	1.03 (.06)	1.15 (.16)	.92 (.13)	.90 (.11)
Thigh	Adult male	9.70 (1.81)	9.69 (1.22)	10.90 (1.07)	10.34 (1.01)	10.90 (1.36)	9.69 (1.15)
	Male swimmers	10.49 (1.96)	10.23 (1.30)	11.92 (1.40)	10.70 (1.15)	11.06 (1.30)	9.65 (1.45)
	Female swimmers	8.06 (1.72)	8.83 (.86)	8.94 (.77)	9.03 (.76)	9.68 (1.01)	8.11 (.63)
Shank	Adult male	3.12 (.28)	4.03 (.55)	3.30 (.33)	3.61 (.43)	3.39 (.48)	3.46 (.44)
	Male swimmers	3.37 (.37)	4.32 (.629)	3.63 (.40)	3.81 (.45)	3.56 (.61)	3.58 (.51)
	Female swimmers	2.58 (.19)	3.31 (.44)	2.79 (.24)	3.00 (.36)	2.60 (.43)	2.92 (.33)

(C) Chandler model; (Y) Yeardon model; (Z1) Zatsiorsky simple regression model; (Z2) Zatsiorsky multiple regression model; (Z3) Zatsiorsky geometric model (Z3); (DXA) and the proposed estimation protocol using DXA.

Table 7. Mean (SD) distance of the centre of mass position in the longitudinal axis from the distal end point (COM, cm) of adult Caucasian male ($n = 10$), male swimmers ($n = 10$) and female swimmers ($n = 8$).

Segment	Group	Estimation Method					
		C	Y	Z1	Z2	Z3	DXA
Head	Adult male	11.91 (.86)	11.81 (1.21)	11.88 (1.68)	14.77 (1.31)	12.05 (.87)	11.32 (.88)
	Male swimmers	13.04 (8.72)	11.94 (.86)	13.98 (1.42)	15.48 (1.80)	13.19 (.73)	11.57 (.55)
	Female swimmers	12.01 (.86)	11.14 (.92)	12.12 (1.80)	15.15 (.54)	12.15 (.87)	11.69 (.31)
Trunk	Adult male	35.70 (.92)	27.29 (.839)	26.18 (.55)	28.42 (1.32)	28.36 (.73)	27.96 (1.08)
	Male swimmers	37.89 (1.32)	30.27 (.99)	28.47 (1.21)	31.94 (1.11)	30.11 (1.05)	30.81 (.89)
	Female swimmers	34.47 (1.62)	26.48 (1.13)	24.78 (1.38)	27.16 (1.13)	27.39 (1.29)	27.02 (.89)
Head + Trunk	Adult male	39.10 (.87)	32.71 (1.23)	32.12 (.65)	34.87 (1.71)	34.73 (.97)	33.74 (1.27)
	Male swimmers	41.44 (1.30)	35.27 (1.15)	34.72 (1.18)	38.55 (1.44)	36.20 (.97)	36.39 (.99)
	Female swimmers	38.09 (1.63)	31.44 (1.32)	31.51 (1.51)	33.92 (1.15)	33.91 (1.40)	33.06 (.89)
Upper arm	Adult male	14.68 (.85)	15.78 (.94)	16.19 (1.59)	13.26 (.72)	12.56 (.73)	15.28 (.829)
	Male swimmers	15.76 (1.19)	17.20 (1.20)	17.74 (1.88)	14.10 (1.04)	13.48 (1.02)	16.18 (1.43)
	Female swimmers	14.68 (.73)	16.02 (.74)	16.79 (1.20)	13.38 (.64)	12.56 (.63)	15.26 (.52)
Forearm	Adult male	14.93 (1.16)	14.79 (1.29)	11.03 (1.58)	9.97 (.82)	13.87 (1.08)	15.40 (1.23)
	Male swimmers	15.77 (1.32)	15.49 (1.28)	11.86 (1.85)	10.46 (.92)	14.65 (1.23)	16.46 (1.51)
	Female swimmers	14.47 (.97)	14.10 (.89)	10.22 (1.33)	9.43 (.72)	13.44 (.90)	14.86 (1.01)
Thigh	Adult male	26.38 (1.92)	24.06 (1.75)	19.21 (2.08)	22.23 (2.38)	25.74 (1.88)	24.42 (1.75)
	Male swimmers	27.21 (2.15)	24.84 (1.96)	19.23 (2.59)	23.13 (2.42)	26.55 (2.10)	24.80 (2.20)
	Female swimmers	26.19 (1.59)	24.51 (1.61)	19.91 (1.92)	22.39 (2.32)	25.56 (1.55)	23.85 (1.35)
Shank	Adult male	24.36 (1.74)	24.09 (1.75)	25.38 (2.17)	26.34 (1.81)	23.01 (1.65)	24.49 (1.75)
	Male swimmers	25.74 (1.91)	25.50 (2.19)	26.81 (2.56)	27.82 (2.12)	24.32 (1.80)	25.72 (2.23)
	Female swimmers	23.72 (1.72)	23.28 (1.64)	24.32 (2.24)	25.48 (1.69)	22.40 (1.62)	23.66 (1.56)

(C) Chandler model; (Y) Yeadon model; (Z1) Zatsiorsky simple regression model; (Z2) Zatsiorsky multiple regression model; (Z3) Zatsiorsky geometric model (Z3); (DXA) and the proposed estimation protocol using DXA.

The %RMSE of mass, COM and I_{xx} of each indirect method, when compared with DXA for each group, are reported in Tables 9, 10 and 11, respectively. In general, greatest errors were observed when indirect methods were used to estimate I_{xx} . In contrast, estimation of COM produced the least errors when using any of the indirect estimation methods. Error assessment of all indirect BSIP methods by subject group was presented by plotting the

MAPE for mass (Figure 6), COM (Figure 7) and I_{xx} (Figure 8).

The SPANOVAs showed significant estimation method by subject group interactions in absolute errors for all segment masses, except for the head (trunk mass: $F(6.99,87.41) = 5.15$; head + trunk mass: $F(7.03,87.91) = 8.42$; upper arm mass: $F(3.69,97.76) = 3.10$; forearm mass: $F(4.71,124.90) = 3.78$; thigh mass: $F(5.83,154.44)$

Table 8. Mean (SD) values for segment principal moment of inertia about the sagittal axis (I_{xx} , $\text{Kg}\cdot\text{cm}^2$) of adult Caucasian male ($n = 10$), male swimmers ($n = 10$) and female swimmers ($n = 8$).

Segment	Group	Estimation Method					
		C	Y	Z1	Z2	Z3	DXA
Head	Adult male	248.95 (69.14)	226.92 (71.57)	280.09 (19.65)	400.67 (84.37)	366.98 (84.27)	233.51 (46.15)
	Male swimmers	290.75 (61.00)	230.10 (54.30)	299.95 (22.06)	441.04 (93.48)	372.79 (94.18)	253.81 (29.45)
	Female swimmers	226.96 (25.79)	141.22 (40.58)	259.11 (15.72)	379.78 (33.37)	309.98 (63.34)	197.83 (19.44)
Trunk	Adult male	16595 (2574)	14501 (1887)	13523 (1474)	16841 (1599)	13142 (1762)	13239 (1838)
	Male swimmers	20324 (4133)	20276 (3150)	16551 (2461)	21743 (2861)	17157 (2750)	17959 (2774)
	Female swimmer	12014 (2222)	10938 (1725)	9868 (1101)	13467 (1916)	10096 (1534)	10728 (1553)
Head + Trunk	Adult male	21522 (2884)	22758 (3521)	22446 (2496)	27680 (3254)	22119 (2989)	21123 (2918)
	Male swimmers	26264 (4647)	29056 (4717)	27356 (3300)	33511 (4081)	27531 (3883)	27198 (3871)
	Female swimmers	16263 (2455)	16725 (2784)	17969 (1661)	23286 (2840)	17373 (2225)	17510 (2253)
Upper arm	Adult male	167.92 (42.42)	194.90 (48.10)	135.71 (21.56)	205.55 (28.37)	133.72 (30.94)	161.64 (35.41)
	Male swimmers	230.29 (63.78)	266.42 (75.58)	157.93 (24.67)	241.06 (34.00)	166.40 (49.98)	207.70 (65.86)
	Female swimmer	142.30 (27.14)	167.27 (32.75)	109.70 (16.86)	186.09 (20.74)	98.50 (17.29)	125.88 (18.88)
Forearm	Adult male	56.33 (17.31)	67.80 (18.52)	68.42 (8.77)	78.17 (18.64)	63.22 (23.62)	64.25 (19.20)
	Male swimmers	70.52 (23.18)	86.30 (28.89)	77.16 (10.75)	92.46 (23.84)	79.11 (27.19)	75.81 (23.61)
	Female swimmer	42.22 (11.75)	53.24 (16.11)	54.79 (6.52)	64.25 (16.40)	45.92 (12.25)	44.62 (12.25)
Thigh	Adult male	2072 (592)	1538 (428)	2149 (347)	1618 (303)	1867 (404)	1531 (369)
	Male swimmers	2316 (583)	1721 (446)	2500 (411)	1742 (362)	1975 (418)	1552 (451)
	Female swimmer	1779 (357)	1357 (260)	1666 (264)	1309 (210)	1602 (250)	1178 (185)
Shank	Adult male	519 (148)	633 (184)	418 (80)	458 (108)	494 (147)	449 (123)
	Male swimmers	619 (165)	759 (208)	502 (89)	527 (103)	576 (157)	516 (140)
	Female swimmer	396 (101)	489 (124)	334 (64)	376 (103)	363 (112)	362 (98)

(C) Chandler model; (Y) Yeadon model; (Z1) Zatsiorsky simple regression model; (Z2) Zatsiorsky multiple regression model; (Z3) Zatsiorsky geometric model (Z3); (DXA) and the proposed estimation protocol using DXA.

Table 9. Percentage Root Mean Square Error (%RMSE) for segment mass (Kg) observed for adult Caucasian male ($n = 10$), male swimmers ($n = 10$) and female swimmers ($n = 8$).

Segment	Group	Estimation Method				
		C	Y	Z1	Z2	Z3
Head	Adult male	13.97	12.99	8.37	23.69	17.44
	Male swimmers	12.66	7.83	4.68	25.47	14.50
	Female swimmers	11.50	15.50	12.06	30.36	14.76
Trunk	Adult male	16.69	4.94	3.87	8.57	6.49
	Male swimmers	10.60	3.00	9.99	5.17	7.06
	Female swimmers	15.75	4.69	6.72	11.20	9.41
Head + Trunk	Adult male	13.04	5.20	3.32	9.46	4.10
	Male swimmers	7.99	3.18	8.40	2.80	4.96
	Female swimmers	12.20	5.82	4.61	13.31	6.57
Upper arm	Adult male	13.47	9.80	13.04	13.58	7.58
	Male swimmers	16.88	13.02	15.40	13.87	6.31
	Female swimmers	8.20	12.08	13.38	20.27	8.71
Forearm	Adult male	11.20	12.93	9.24	16.90	15.79
	Male swimmers	9.60	12.40	7.74	15.65	9.24
	Female swimmers	19.57	16.95	17.46	28.36	7.27
Thigh	Adult male	16.45	4.42	13.53	10.47	13.89
	Male swimmers	19.81	7.27	24.92	13.48	16.61
	Female swimmers	19.36	10.40	10.97	13.23	20.42
Shank	Adult male	12.32	17.01	8.78	6.81	5.65
	Male swimmers	7.50	21.13	6.50	8.42	5.60
	Female swimmers	13.24	17.82	8.62	10.64	17.24

(C) Chandler model; (Y) Yeadon model; (Z1) Zatsiorsky simple regression model; (Z2) Zatsiorsky multiple regression model;(Z3) Zatsiorsky geometric model (Z3).

= 8.72; shank mass: $F(5.94,157.31) = 4.16$). For COM, the thigh was the only segment where significant estimation method by subject group interaction was observed ($F(3.17,84.11) = 4.39$). No significant interactions occurred for the head, and the head + trunk segments between the estimation method and subject group for segment I_{xx} , (trunk I_{xx} : $F(5.72,71.47) = 3.32$; upper arm I_{xx} : $F(4.41,116.98) = 4.43$; forearm I_{xx} : $F(5.99,158.76) = 4.25$; thigh I_{xx} : $F(5.31,140.63) = 6.92$; shank I_{xx} : $F(5.82,154.33) = 2.19$).

The SPANOVAs also revealed differences ($p < 0.05$) in absolute errors between estimation methods for all BSIPs; whereas differences between subject groups were found for trunk mass ($F(2,25) = 15.17$), head + trunk mass ($F(2,25) = 33.50$), forearm mass ($F(2,53) = 6.80$), thigh mass ($F(2,53) = 6.80$), head and trunk I_{xx} ($F(2,25) = 3.48$), upper arm I_{xx} ($F(2,53) = 4.58$), forearm I_{xx} ($F(2,53) = 4.40$) and thigh I_{xx} ($F(2,53) = 7.00$). The Tukey HSD post hoc test indicated greater errors within female swimmers than the other two groups for trunk mass, head

Table 10. Percentage Root Mean Square Error (%RMSE) for segment centre of mass position in the longitudinal axis from the distal end point (COM, cm) observed for adult Caucasian male ($n = 10$), male swimmers ($n = 10$) and female swimmers ($n = 8$).

Segment	Group	Estimation Method				
		C	Y	Z1	Z2	Z3
Head	Adult male	10.86	11.74	15.73	32.62	11.65
	Male swimmers	14.27	8.26	23.71	38.04	15.50
	Female swimmers	8.11	9.02	15.31	30.49	8.68
Trunk	Adult male	28.06	3.09	7.35	3.45	3.45
	Male swimmers	23.10	2.24	8.48	4.42	2.98
	Female swimmers	27.74	3.17	8.92	3.04	2.88
Head + Trunk	Adult male	16.36	3.88	6.04	4.35	3.93
	Male swimmers	14.02	3.20	5.41	6.68	1.98
	Female swimmers	15.43	5.53	5.58	3.70	3.87
Upper arm	Adult male	5.67	5.89	9.97	13.66	18.11
	Male swimmers	3.61	7.28	10.42	12.95	16.72
	Female swimmers	5.14	6.17	11.87	12.70	17.92
Forearm	Adult male	4.30	5.18	29.26	35.30	10.30
	Male swimmers	5.07	6.29	28.85	36.48	11.26
	Female swimmers	3.43	5.80	31.83	36.56	9.74
Thigh	Adult male	8.52	2.71	21.86	10.34	6.09
	Male swimmers	10.16	2.48	23.24	7.85	7.61
	Female swimmers	10.02	3.62	17.36	8.49	7.43
Shank	Adult male	1.66	2.36	4.38	7.81	6.21
	Male swimmers	2.40	1.83	5.74	8.76	5.81
	Female swimmers	2.41	2.67	4.44	7.77	5.80

(C) Chandler model; (Y) Yeadon model; (Z1) Zatsiorsky simple regression model; (Z2) Zatsiorsky multiple regression model;(Z3) Zatsiorsky geometric model (Z3).

Table 11. Percentage Root Mean Square Error (%RMSE) for segment principal moment of inertia about the sagittal axis (I_{xx} , $\text{Kg}\cdot\text{cm}^2$) observed for adult Caucasian male ($n = 10$), male swimmers ($n = 10$) and female swimmers ($n = 8$).

Segment	Group	Estimation Method				
		C	Y	Z1	Z2	Z3
Head	Adult male	19.25	24.24	29.84	76.86	59.87
	Male swimmers	26.00	18.75	20.48	82.82	57.48
	Female swimmers	23.13	32.63	33.96	97.50	63.43
Trunk	Adult male	29.33	12.82	6.20	29.07	6.07
	Male swimmers	15.24	13.85	11.10	22.63	6.74
	Female swimmers	15.98	7.61	9.19	27.19	9.14
Head + Trunk	Adult male	8.52	12.78	7.93	32.17	6.63
	Male swimmers	7.29	9.23	5.06	24.49	4.30
	Female swimmers	9.60	9.49	6.70	33.84	6.03
Upper arm	Adult male	14.98	26.91	18.00	33.59	19.57
	Male swimmers	18.28	33.55	24.16	30.99	20.43
	Female swimmers	18.46	36.61	15.14	50.81	22.51
Forearm	Adult male	16.60	13.96	23.75	31.93	20.13
	Male swimmers	12.00	17.53	23.05	27.41	13.84
	Female swimmers	10.17	22.63	33.80	46.85	12.59
Thigh	Adult male	37.23	9.05	45.54	17.91	27.39
	Male swimmers	52.30	14.85	72.90	21.23	34.25
	Female swimmers	52.33	17.58	42.55	19.81	40.20
Shank	Adult male	16.30	41.24	13.40	8.35	12.30
	Male swimmers	22.96	49.55	11.89	10.82	16.74
	Female swimmers	19.09	40.95	16.25	19.87	25.35

(C) Chandler model; (Y) Yeadon model; (Z1) Zatsiorsky simple regression model; (Z2) Zatsiorsky multiple regression model; (Z3) Zatsiorsky geometric model (Z3).

+ trunk mass, and forearm mass ($p < 0.05$). Also, they recorded greater errors than male swimmers for forearm I_{xx} , and normal male subjects for upper arm I_{xx} ($p < 0.05$). The non-swimmers revealed lower errors than male and female swimmers, for head + trunk mass, thigh mass ($p < 0.05$) and thigh I_{xx} than male swimmers; while tending towards lower errors ($p = 0.056$) than female swimmers. Although significant differences were found between

groups for the head + trunk I_{xx} , the Tukey HSD did not indicate which pairs were different.

Discussion

Primarily, this study sought to validate BSIP data extracted from DXA scans and then compared DXA with five other indirect BSIP methods, using 10 elite male and

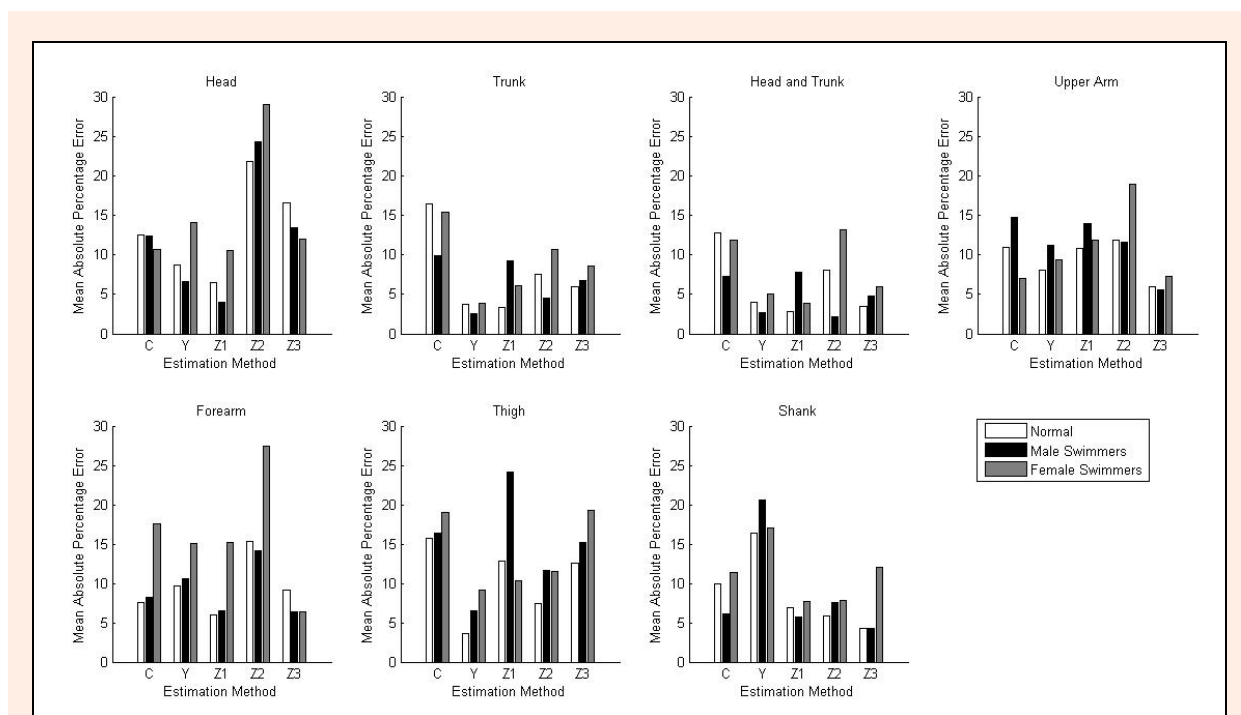


Figure 6. Mean Absolute Percentage Error (MAPE) for segment mass (Kg) observed for young adult Caucasian males (Normal), Male swimmers and Female swimmers.

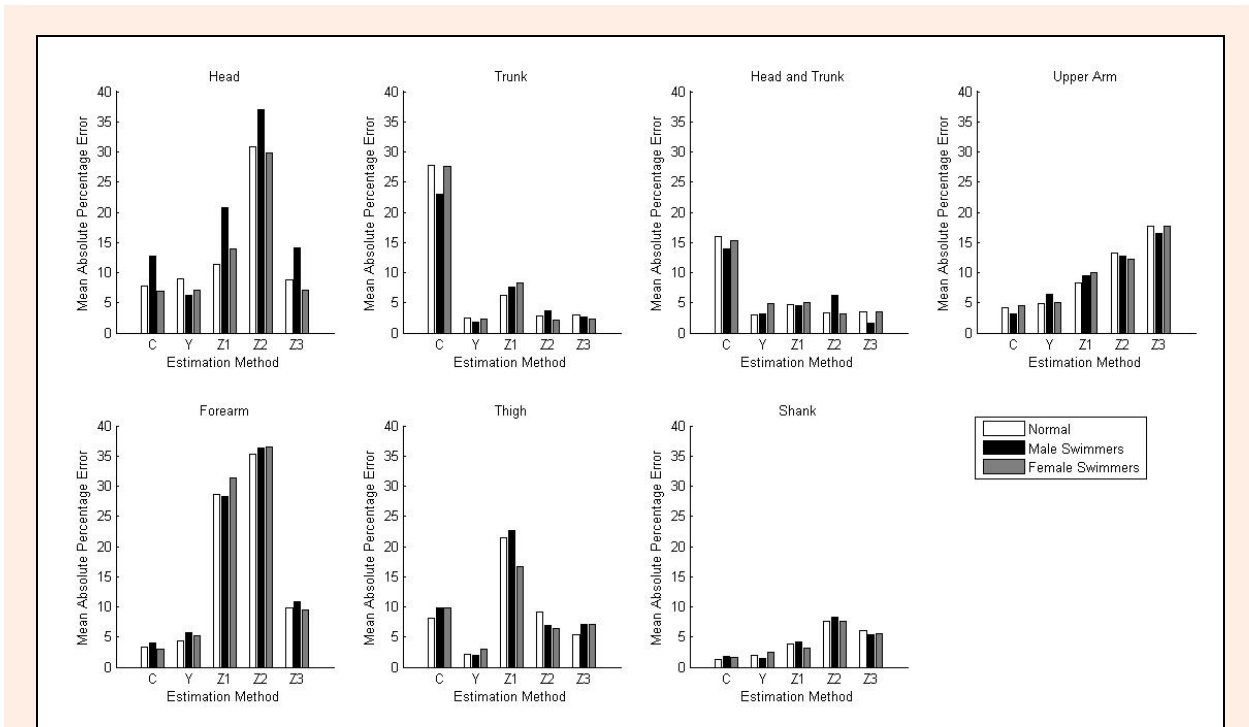


Figure 7. Mean Absolute Percentage Error (MAPE) for segment center of mass position in the longitudinal axis from the distal end point (COM, cm) observed for young adult Caucasian males (Normal), Male swimmers and Female swimmers.

8 elite female swimmers, and 10 young adult Caucasian males as subjects. In previous studies, the DXA relied on the relationships between the attenuation coefficients of the high energy beams and the mass of a given phantom to predict the mass of the scanned object (Durkin et al., 2002). A unique feature of this study was that the mass

value for each unit area (mass element) could be extracted directly, via authorization from the manufacturer, Healthcare Division of General Electric Company (GEHC). Their enCORE[®] software also can export two bitmap images to graphically illustrate mass distribution within the scanned area. Because the software did not allow mass

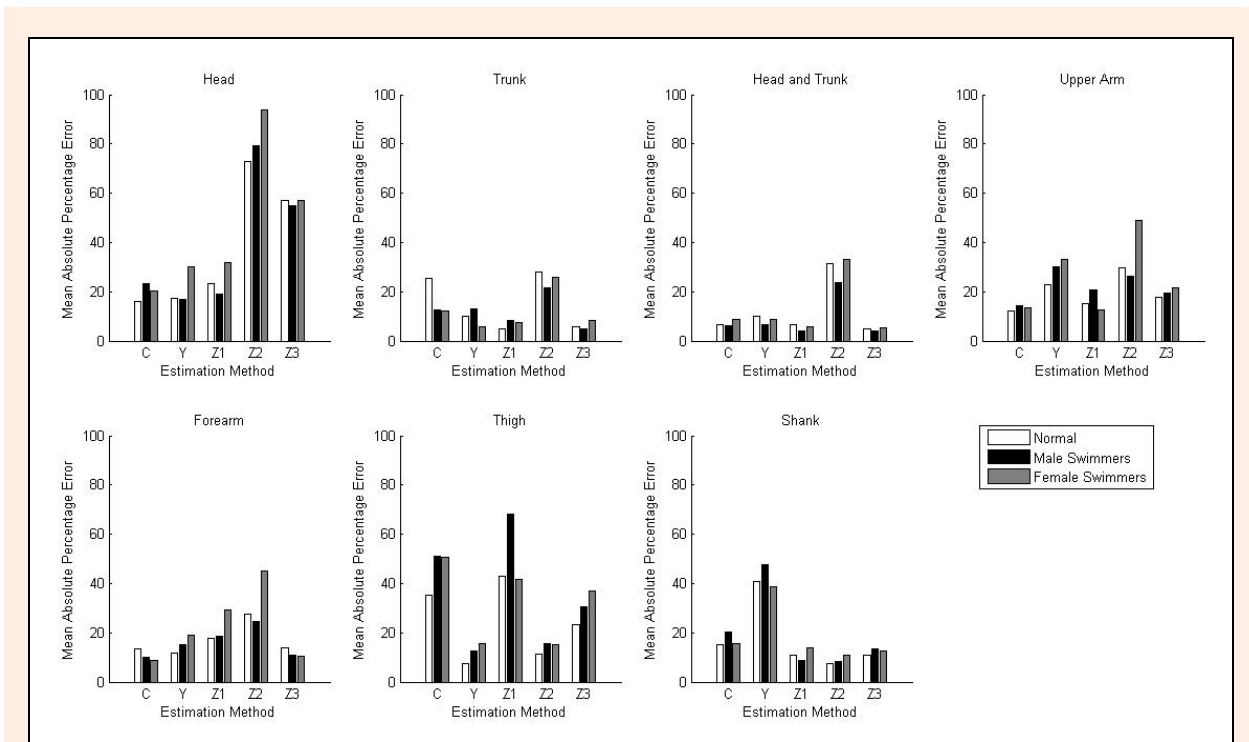


Figure 8. Mean Absolute Percentage Error (MAPE) for segment principal moment of inertia about the sagittal axis (I_{xx} , Kg·cm²) observed for young adult Caucasian males (Normal), Male swimmers and Female swimmers.

element data to be exported into any other formats, it was necessary to establish the relationship between mass elements and the pixel intensity of the scan images. The comparison between segment mass calculated from pixel color-mass relationship and the mass calculated for the two compartments (BM mass and tissue mass) by the enCORE[®] software revealed a similar level of accuracy as found previously (Durkin et al., 2002). The lower accuracy of the bone mineral mass seemed to result from inadequate threshold values used to create the binary images of the bone mineral images. When comparing both the noise and noise-free images, some bone information could have been lost. The edges of several flat bones did not line up with the edges of the rectangular mass elements (Wicke and Dumas, 2008) and could have contributed to errors in bone mass values for pixels closest to the boundaries of those bones.

Also, BSIP profiles of elite swimmers were different ($p < 0.05$) from those of untrained Caucasian adults (Tables 6, 7 and 8). Durkin and Dowling (2003) urged caution with subjects not reasonably matched to those whom the equations were devised. When compared with the DXA method used here, the 5 indirect BSIP estimations for the 10 non-athletes also consistently produced more errors (Tables 9, 10 and 11). Figure 6 illustrates that none of the 5 indirect estimation methods consistently reported MAPEs less than 5%. This was despite subjects approximating the anatomical features of the subjects from *y* Zatsiorsky and Seluyanov (Zatsiorsky and Seluyanov, 1983; 1985).

Absolute and relative body sizes, somatotypes and body compositions of elite swimmers are different from those of a normal untrained population (Ackland et al., 2009). Furthermore, Carter and Ackland (1994) reported that anatomical characteristics of elite swimmers also vary with genders and swim events (strokes and distances). Therefore, perhaps one could expect that equations using just the whole body mass, or mass and stature (C and Z1), would result in greater MAPE values. However, our results showed that the Z2 model, which used the greatest number of anthropometric variables as predictors, also had large errors ($> 20\%$) and varied greatly between groups (Figures 6, 7 and 8). The geometric models (Y and Z3) seemed to generate less error in general. However, none of the latter consistently performed better than the others. Even though Y appeared to resemble the geometric shape of the body better than Z3, using uniform segment densities gathered from cadavers might have contributed to the errors found. The Z3 method uses a quasi-density value to compensate for differences between the actual segment volume and its cylindrical representation. This approach, however, was not enough to provide low and consistent levels of MAPE between the groups for all segments and, especially, was more evident for the lower limbs. For most of the body segments, results of this study reject the hypothesis that the indirect methods would produce significantly lower errors for the untrained adult group than the two athlete groups. The hypothesis was based on the premise that the indirect method would only be accurate for subjects with similar anthropometric profiles to the population from which the

method was developed. The normal young adults tested in this study closely resembled the population used to develop Z1, Z2 and Z3 (Zatsiorsky and Seluyanov, 1983; 1985; Zatsiorsky et al., 1990). However, errors in the BSIPs estimated for this group using Z1, Z2 and Z3 did not produce consistently less errors than in the elite male and female swimmers. Reduced errors were only found for the thigh and head + trunk segments. Durkin and Dowling (2003) also found similar %RMSE in young adult males which indicated that not even the apparent anatomical similarities minimized the errors yielded by those methods.

Analysis of the COM of the thigh segment revealed a significant interaction between the estimation method and subject group, but no significant differences were found between groups. Good consistency can be observed when plotting the MAPE for COM (Figure 7), as the three groups recorded similarly low errors for most COM and estimation methods. Nevertheless, no estimation method found MAPE to be less than 5% for all COMs, and all groups. The Y method was the only one not showing errors greater than 15% at least once. Also, the greatest %RMSE for Y was 11.74% (Table 10), which was for the head segment of the untrained subjects. This indicated that the uniform density assumption, and the geometrical solids that were used, enabled fairly accurate results for COM estimation. The two methods, C and Z3, used a fixed proportion between COM distance from distal endpoint and segment length. The Chandler method (C) performed poorly for the head, trunk, and head + trunk. Perhaps this could be explained partially by the different segmentation protocol used by Chandler *et al.* (1975). Moreover, once elderly cadavers are used, there needs to be some consideration of the ageing effect over the spine. Over the years, the spine tends to shorten its longitudinal length due to disc flattening when losing the nucleus pulposus from the middle of the spinal disc. Thus, the resultant shorter trunk length might have induced errors when being compared with younger subjects with spines unaffected in this way. The Z3 method used adjusted positions for the COM relative to the joint centers (De Leva, 1996), rather than the anatomical landmarks. However, rather than using the same cohort as Zatsiorsky and colleagues (Zatsiorsky and Seluyanov, 1983; 1985; Zatsiorsky et al., 1990), some adjustments were carried out using anthropometric data from other Caucasian ethnic groups, which certainly added errors to the adjustment. The other two methods (Z1 and Z2) demonstrated considerably large errors for the head, forearm and thigh COMs, although little difference between groups was observed.

The largest percentage errors (MAPE and %RMSE) were found for I_{xx} (Figure 8). Even though I_{xx} does not require mass and COM values for its calculation, it is physically related to those two inertial parameters. Thus, results for I_{xx} were similar to those of mass values where significant interactions between the estimation method and subject group were found for most segments. This was true except for the head, and the head + trunk segments. The I_{xx} for all limb segments of female swimmers seemed to be affected more than in the other two

groups. Even though this was hypothesized, only the thigh segment showed a trend towards having significantly lower percentage errors for the normal subjects, when they were compared with the two groups of swimmers. But, the %RMSE was less than 10% only for the Y method (Table 11). Nevertheless, with %RMSE of up to 50% for the indirect estimation methods, regardless of subject group (Table 11), one should avoid indirect estimation methods when applied to a population of different morphology and body composition from which it was derived.

A limitation of research designs with elite athletes is to find sufficient participants to yield statistically significant differences between groups. Despite the low number of subjects in this study, it was clearly demonstrated that indirect estimation methods failed to provide subject-specific BSIP data. Furthermore, in a within-group research designs, the sample mean is used as a representative value of the group. Thus, it could mask important information of some individuals. Therefore, when dealing with elite level athletes, research needs to focus on an individual athlete for an accurate assessment of performance or any effects of an intervention (Kinugasa et al., 2004). This is another reason why subject-specific BSIP estimation methods should be preferred over indirect estimation methods.

Despite accuracy, easy access, low radiation exposure and easier data processing than required for other medical imaging technologies, there are limitations that prevent DXA from being used for BSIP calculations. One limitation is that one might not be able to access the raw data as this function is not readily available in the software, possibly due to concerns relating to intellectual property by the manufacturers. Furthermore, the DXA scan table may not be large enough for elite swimmers or athletes from other sports as they are generally much taller and larger than populations for which DXA was designed. The scanner used in this study has a scan area of 59.75cm x 197cm, which was slightly larger than the machine used in previous studies (Hologic QDR-1000/W 59.4cm x 192.7cm, Hologic Inc., Bedford, MA, USA) (Durkin and Dowling, 2003; 2006; Durkin et al., 2002;2005). A major limitation of DXA lies in its 2D characteristics of the results. Hence, it does not allow calculations of the COM position in the sagittal plane, and the principal moments of inertia about the longitudinal and transverse axes (Durkin et al., 2002; Ganley and Powers, 2004b; Wicke and Dumas, 2008). Therefore, kinetic analyses in sporting maneuvers that are typically three-dimensional (e.g., swimming) cannot rely on data extracted from DXA without incorporating other modeling techniques. Several modeling technique approaches can be performed, as proposed in previous studies (Durkin and Dowling, 2006; Durkin et al., 2005; Lee et al., 2009; Wicke et al., 2008; 2009).

Finally, it can be argued that the influence of errors in BSIP calculations depends on the nature of the movement being analyzed. Factors such as whether the task involves rapid linear/angular movements of the segments, is an open-chain or closed-chain analysis, or whether external forces exert greater or lesser influence than the

BSIP method used, will determine the level of accuracy in the joint forces and moments calculated. However, this study demonstrated that using an indirect estimation method can lead to grossly inaccurate BSIPs. The recent advances in kinematic analysis systems have resulted in greater validity, reproducibility, and also flexibility with regard to the environment in which the assessment is required. It seems counter-intuitive then to ignore the potential errors from using inappropriate BSIP data. However, extracting full body 3D BSIP from DXA requires further development before it can be readily used.

Conclusion

Using the M-R1 DXA method, significant differences in BSIPs were observed between 10 young adult Caucasian males, 10 elite male swimmers, and 8 elite female swimmers. Elite female swimmers have significantly lower segment masses than the other groups, and male swimmers had greater inertial measures of the trunk and upper arms than the others. Validation of this method by comparing body mass calculation against output by DXA software revealed errors of less than 1.5%

Using DXA method, this study showed that elite swimmers recorded significantly different BSIPs than young adult Caucasian males, and elite male swimmers reported significantly different BSIPs than elite female swimmers. When using the results of the DXA method as criteria against BSIPs computed using five indirect estimation methods, significant errors were observed in all of the BSIP indirect estimation methods, and none were suitable for any groups, segments or BSIP. Therefore, caution should be taken when computing BSIPs for elite swimmers, and DXA should be used when accessible.

Hence, future studies should investigate errors yielded by indirect BSIPs when applied to other elite sportsmen populations, or outliers in physique types (e.g. obese, elderly, etc); and investigate the influence of inaccurate BSIPs in dynamic analyses of elite athletes. Furthermore, this study demonstrated that DXA can be used to provide accurate BSIPs. However, further development is required to enable estimation of BSIPs in all dimensions.

Acknowledgments

This work was supported by the ARC linkage project LP110100189.

References

- Ackland, T., Henson, P. and Bailey, D. (1988) The uniform density assumption: Its effect upon the estimation of body segment inertial parameters. *International Journal of Sports Biomechanics* **4**, 146-155.
- Ackland, T. R., Elliott, B. and Bloomfield, J. (2009) *Applied Anatomy and Biomechanics in Sport*. Human Kinetics Publishers.
- Besier, T.F., Sturmiels, D.L., Alderson, J. A. and Lloyd, D.G. (2003) Repeatability of gait data using a functional hip joint centre and a mean helical knee axis. *Journal of Biomechanics* **36**, 1159-1168.
- Bixler, B. and Schloder, M. (1996) Computational fluid dynamics: an analytical tool for the 21st century swimming scientist. *Journal of Swimming Research* **11**, 4-22.
- Campbell, A., Lloyd, D., Alderson, J. and Elliott, B. (2009) MRI development and validation of two new predictive methods of glenohumeral joint centre location identification and

- comparison with established techniques. *Journal of Biomechanics* **42**, 1527-1532.
- Carter, J.E.L. and Ackland, T.R. (1994) *Kinanthropometry in Aquatic Sports: a Study of World Class Athletes*, Human Kinetics.
- Ceseracciu, E., Sawacha, Z., Fantozzi, S., Cortesi, M., Gatta, G., Corazza, S. and Cobelli, C. (2011) Markerless analysis of front crawl swimming. *Journal of Biomechanics* **44**, 2236-2242.
- Chandler, R.F., Clauser, C.E., Mcconville, J.T., Reynolds, H.M. and Young, J.W. (1975) *Investigation of inertial properties of the human body. AMRL-TR-70-137*. Ohio: Aerospace Medical Research Laboratory, Wright-Patterson Air Force Base.
- Cheng, C.K., Chen, H.H., Chen, C.S., Lee, C.L. and Chen, C.Y. (2000) Segment inertial properties of Chinese adults determined from magnetic resonance imaging. *Clinical Biomechanics* **15**, 559-566.
- Chin, A., Lloyd, D., Alderson, J., Elliott, B. and Mills, P. (2010) A marker-based mean finite helical axis model to determine elbow rotation axes and kinematics in vivo. *Journal of Applied Biomechanics* **26**, 305-315.
- Clauser, C.E., Mcconville, J.T. and Young, J.W. (1969) *Weight, volume, and center of mass of segments of the human body. AMRL-TL-69-70*. Ohio: Aerospace Medical Research Laboratory, Wright-Patterson Air Force Base.
- De Leva, P. (1996) Adjustments to Zatsiorsky-Seluyanov's segment inertia parameters. *Journal of Biomechanics* **29**, 1223-1230.
- Dempster, W.T. (1955) *Space requirements of the seated operator*. WADC Technical Report 55159 55-159.
- Durkin, J. and Dowling, J. (2006) Body segment parameter estimation of the human lower leg using an elliptical model with validation from DEXA. *Annals of Biomedical Engineering* **34**, 1483-1493.
- Durkin, J.L. (2008) Measurement and estimation of human body segment parameters. In: *Routledge Handbook of Biomechanics and Human Movement Science*. Eds: Hong, Y. and Bartlett, R. Abingdon: Routledge.
- Durkin, J.L. and Dowling, J.J. (2003) Analysis of body segment parameter differences between four human populations and the estimation errors of four popular mathematical models. *Journal of Biomechanical Engineering* **125**, 515-522.
- Durkin, J.L., Dowling, J.J. and Andrews, D.M. (2002) The measurement of body segment inertial parameters using dual energy X-ray absorptiometry. *Journal of Biomechanics* **35**, 1575-1580.
- Durkin, J.L., Dowling, J.J. and Scholtes, L. (2005) Using mass distribution information to model the human thigh for body segment parameter estimation. *Journal of Biomechanical Engineering* **127**, 455-464.
- Ellis, K.J. (2000) Human body composition: in vivo methods. *Physiological Reviews* **80**, 649-680.
- Fuller, N., Laskey, M. and Elia, M. (1992) Assessment of the composition of major body regions by dual energy X ray absorptiometry (DEXA), with special reference to limb muscle mass. *Clinical Physiology* **12**, 253-266.
- Ganley, K.J. and Powers, C.M. (2004a) Anthropometric parameters in children: a comparison of values obtained from dual energy x-ray absorptiometry and cadaver-based estimates. *Gait and Posture* **19**, 133-140.
- Ganley, K.J. and Powers, C.M. (2004b) Determination of lower extremity anthropometric parameters using dual energy X-ray absorptiometry: the influence on net joint moments during gait. *Clinical Biomechanics* **19**, 50-56.
- Haarbo, J., Gottfredsen, A., Hassager, C. and Christiansen, C. (1991) Validation of body composition by dual energy X-ray absorptiometry (DEXA). *Clinical Physiology* **11**, 331-341.
- Hanavan Jr, E.P. (1964) *A mathematical model of the human body. AMRL-TR-64-102, AD-608-463*. Ohio: Aerospace Medical Research Laboratory, Wright-Patterson Air Force Base.
- Huang, H.K. and Suarez, F.R. (1983) Evaluation of cross-sectional geometry and mass density distributions of humans and laboratory animals using computerized tomography. *Journal of Biomechanics* **16**, 821-832.
- Kinugasa, T., Cerin, E. and Hooper, S. (2004) Single-subject research designs and data analyses for assessing elite athletes' conditioning. *Sports Medicine* **34**, 1035-1050.
- Laskey, M.A. (1996) Dual-energy X-ray absorptiometry and body composition. *Nutrition* **12**, 45-51.
- Lee, M.K., Le, N.S., Fang, A.C. and Koh, M.T.H. (2009) Measurement of body segment parameters using dual energy X-ray absorptiometry and three-dimensional geometry: An application in gait analysis. *Journal of Biomechanics* **42**, 217-222.
- Lu, J.M. and Wang, M.J.J. (2008) Automated anthropometric data collection using 3D whole body scanners. *Expert Systems with Applications* **35**, 407-414.
- Lyttle, A. and Keys, M. (2006) The application of computational fluid dynamics for technique prescription in underwater kicking. *Portuguese Journal of Sport Sciences* **6**, 233-235.
- Marinho, D., Barbosa, T., Kjendlie, P., Vilas-Boas, J., Alves, F., Rouboia, A. and Silva, A. (2009) Swimming Simulation: A New Tool for Swimming Research and Practical Applications. In: *Computational Fluid Dynamics for Sport Simulation*. Ed: Peters, M. Heidelberg, Germany: Springer.
- Martin, P.E., Mungiole, M., Marzke, M.W. and Longhill, J.M. (1989) The use of magnetic resonance imaging for measuring segment inertial properties. *Journal of Biomechanics* **22**, 367-376.
- Mazess, R.B., Barden, H.S., Bisek, J.P. and Hanson, J. (1990) Dual-energy x-ray absorptiometry for total-body and regional bone-mineral and soft-tissue composition. *The American Journal of Clinical Nutrition* **51**, 1106-1112.
- Mungiole, M. and Martin, P.E. (1990) Estimating segment inertial properties: Comparison of magnetic resonance imaging with existing methods. *Journal of Biomechanics* **23**, 1039-1046.
- Olds, T.S. and Tomkinson, G.R. (2009) Absolute Body Size. In: *Applied Anatomy and Biomechanics in Sport*. Eds: Ackland, T. R., Elliott, B.C. & Bloomfield, J. Champaign, IL: Human Kinetics. 29-46.
- Rossi, M., El-Sallam, A., Benjanuvatra, N., Lyttle, A., Blanksby, B. and Bennamoun, M. (2012) A novel approach to calculate body segments inertial parameters from DXA and 3D Scanners Data. *4th International Conference on Computational Methods, November 25-27, Gold Coast, Australia*. Book of Abstract. 228.
- St-Onge, M.-P., Wang, J., Shen, W., Wang, Z., Allison, D.B., Heshka, S., Pierson, R.N. and Heymsfield, S.B. (2004) Dual-Energy X-Ray Absorptiometry-measured lean soft tissue mass: differing relation to body cell mass across the adult life span. *The Journals of Gerontology Series A: Biological Sciences and Medical Sciences* **59**, B796-B800.
- Thorpe, J. and Steel, S. (1999) Image resolution of the Lunar Expert-XL. *Osteoporosis International* **10**, 95-101.
- Wicke, J. and Dumas, G.A. (2008) Estimating segment inertial parameters using fan-beam DXA. *Journal of Applied Biomechanics* **24**, 180-184.
- Wicke, J., Dumas, G. A. and Costigan, P. A. (2008) Trunk density profile estimates from dual X-ray absorptiometry. *Journal of Biomechanics* **41**, 861-867.
- Wicke, J., Dumas, G.A. and Costigan, P.A. (2009) A comparison between a new model and current models for estimating trunk segment inertial parameters. *Journal of Biomechanics* **42**, 55-60.
- Wu, G., Van Der Helm, F.C.T., Veeger, H.E.J., Makhssous, M., Van Roy, P., Anglin, C., Nagels, J., Karduna, A.R., Mcquade, K., Wang, X., Werner, F.W. and Buchholz, B. (2005) ISB recommendation on definitions of joint coordinate systems of various joints for the reporting of human joint motion—Part II: shoulder, elbow, wrist and hand. *Journal of Biomechanics* **38**, 981-992.
- Yeadon, M. (1990) The simulation of aerial movement—II. A mathematical inertia model of the human body. *Journal of Biomechanics* **23**, 67-74.
- Yeadon, M. R. and Morlock, M. (1989) The appropriate use of regression equations for the estimation of segmental inertia parameters. *Journal of Biomechanics* **22**, 683-689.
- Zatsiorsky, V. (1983) Biomechanical characteristics of the human body. In: *Biomechanics and Performance in Sport*. Ed: Baumann, W. Schorndorf: Karl Hofmann Verlag. 71-83.
- Zatsiorsky, V. and Seluyanov, V. (1983) The mass and inertia characteristics of the main segments of the human body. In: *Biomechanics VIII-B*. Eds: Matsui, H. and Kobayashi, K. Champaign, IL: Human Kinetics. 1152-1159.
- Zatsiorsky, V. and Seluyanov, V. (1985) Estimation of the mass and inertia characteristics of the human body by means of the best predictive regression equations. In: *Biomechanics IX-B*. Ed: Winter, D. Champaign, IL: Human Kinetics. 233-239.
- Zatsiorsky, V., Seluyanov, V. and Chugunova, L. (1990) In vivo body segment inertial parameters determination using a gamma-scanner method. In: *Biomechanics of Human Movement*:

Applications in Rehabilitation, Sports and Ergonomics. Eds: Berme, N. and Cappozzo, A. Bertec, Ohio. 186-202.

Key points

- Elite swimmers have significantly different body segment inertial parameters than young adult Caucasian males.
- The errors computed from indirect BSIP estimation methods are large regardless whether applied to elite swimmers or young adult Caucasian males.
- No indirect estimation method consistently performed best.

AUTHORS BIOGRAPHY



Marcel ROSSI

Employment

The University of Western Australia, Perth, Australia

Degree

MSc

Research interests

Sports biomechanics, camera calibration, modelling, body segment inertial parameters.

E-mail: 20676873@student.uwa.edu.au



Andrew LYTTLE

Employment

A Senior Sports Biomechanist, Western Australian Institute of Sport

Degree

PhD

Research interests

Swimming biomechanics

E-mail: alyttle@wais.org.au



Amar EL-SALLAM

Employment

Assistant Professor at the University of Western Australia.

Degree

PhD

Research interests

Signal and image processing, computer vision and their applications in sports science

E-mail: elsallam@csse.uwa.edu.au



Nat BENJANUVATRA

Employment

Biomechanics, Motor Learning and Control at the School of Sport Science, Exercise and Health, The University of Western Australia

Degree

PhD

Research interests

Biomechanics and skill acquisition in swimming

E-mail: nat.benjanuvatrat@uwa.edu.au



Brian BLANKSBY

Employment

Head of the School of Sport Science, Exercise and Health, The University of Western Australia, Perth, Australia

Degree

PhD

Research interests

Aquatics

E-mail: brian.blanksby@uwa.edu.au

✉ Marcel Mourao Rossi

School of Sport Science, Health & Exercise Science, The University of Western Australia, 35 Stirling Hwy, Crawley WA 6009, Australia